Impedance Analysis of MDCK Cells Measured by Electric Cell-Substrate Impedance Sensing

Chun-Min Lo, Charles R. Keese, and Ivar Giaever
Department of Physics and Biology, School of Science, Rensselaer Polytechnic Institute, Troy, New York 12180-3590 USA

ABSTRACT Transepithelial impedance of Madin–Darby canine kidney cell layers is measured by a new instrumental method, referred to as electric cell-substrate impedance sensing. In this method, cells are cultured on small evaporated gold electrodes, and the impedance is measured in the frequency range 20–50,000 Hz by a small probing current. A model for impedance analysis of epithelial cells measured by this method is developed. The model considers three different pathways for the current flowing from the electrode through the cell layer: (1) in through the basal and out through the apical membrane, (2) in through the lateral and out through the apical membrane, and (3) between the cells through the paracellular space. By comparing model calculation with experimental impedance data, several morphological and cellular parameters can be determined: (1) the resistivity of the cell layer, (2) the average distance between the basal cell surface and substratum, and (3) the capacitance of apical, basal, and lateral cell membranes. This model is used to analyze impedance changes on removal of Ca^{2+} from confluent Mardin–Darby canine kidney cell layers. The method shows that reduction of Ca^{2+} concentration causes junction resistance between cells to drop and the distance between the basal cell surface and substratum to increase.

INTRODUCTION

Epithelial cells usually form a barrier sheet and exhibit polarity in tissue culture, as the apical cell membranes are connected and sealed with tight junctions (Fromter and Diamond, 1972; Powell, 1981; Gumbiner, 1987; Cereijido et al., 1988; Madara, 1988; Stevenson et al., 1988a). An important function in epithelia is ion permeation, and, of the three major pathways, two are transcellular (through basal and apical membranes or through lateral and apical membranes) and one is paracellular (through intercellular space and tight junction) (Fromter, 1972; Clausen et al., 1979; Boulpaep and Sackin, 1980). A common method to study the ion transport property of epithelial cells is to measure transepithelial resistance by using direct current (dc) (Cereijido et al., 1978; Gumbiner and Simons, 1986; Conyers et al., 1990), but a simple and accurate alternating current (ac) method to measure transepithelial impedance would be useful for studying epithelial transport and morphology. It is relatively simple to construct an equivalent electrical circuit of epithelia by using the dc rather than the ac technique, and there are several methods to estimate tight junctional resistance from the equivalent circuit (Claude, 1978; Lewis and Diamond, 1976; Reuss, 1991). Ac techniques can, however, provide additional information on both resistive and capacitive properties of cell membranes because a membrane can be modeled electrically as a capacitor and a resistor connected in parallel (Lim et al., 1984; Wills and Clausen, 1987; Pappenheimer, 1987). In general, the specific capacitance of cell membranes is approximately 1 $\mu F/cm^2$ (Cole, 1968) but can appear to be much larger if the membrane is folded. A common ac technique is to measure transepithelial impedance with the cell cultured on a membrane in a modified Ussing chamber. The voltage appearing across the cell layers in response to impressed ac currents is measured as a function of time or frequency. Impedance analysis and curve fitting to obtain the electrical values of cell membranes are based on equivalent circuits with lumped or distributed circuit parameters (Madara and Pappenheimer, 1987; Clausen, 1989; Gordon et al., 1989).

Our laboratory has developed a new instrumental method named electric cell-substrate impedance sensing (ECIS) to detect cell motion and morphology in tissue culture (Giaever and Keese, 1984, 1986, 1993). In one application a small current at a chosen frequency is applied to the electrode, and the device monitors the impedance of a cell-covered electrode by using a lock-in amplifier that returns both magnitude and phase of the voltage as a function of time. The data obtained can be related to morphological changes of the cells, and these have been demonstrated to be related to metabolic activities within the small population of cells on the electrode (Giaever and Keese, 1991; Lo et al., 1993). In another application that is used in this paper, ECIS can determine the impedance at various frequencies by scanning an electrode blanketed with confluent cell layers. By analyzing the impedance as a function of frequency, one can develop a model that relates the observed impedance to relevant cell parameters (Giaever and Keese, 1991, 1993). We have successfully obtained morphological information on fibroblastic cells by comparing the calculated impedance values with those measured by ECIS, using two adjustable independent parameters, namely, α and R_b (R_b is the resistivity of the cell layer and $\alpha = r_c(\rho/h)^{1/2}$, where r_c is the effective radius of the spread cell, ρ the resistivity of the solution, and h the average

Received for publication 16 March 1995 and in final form 1 September 1995

Address reprint requests to Dr. Ivar Giaever, Department of Physics and Biology, School of Science, Rensselaer Polytechnic Institute, Troy, NY 12180-3590. Tel.: 518-276-6429; Fax: 518-276-2825; E-mail: usergapk@rpits.mts.

0006-3495/95/12/2800/08 $2.00

distance between the cells and the substratum; see the list of variables in the Appendix). For instance, the confluent cell layer resistance (R_b) of WI-38 and WI-38 VA13 cells is 0.7 and 2.2 $\Omega \cdot cm^2$ respectively, and the average channel height (h) between ventral cell surface and substratum is 113 and 13 nm, respectively, in the two cases.

We have extended the model to be more applicable to epithelial cells. In the simple model the current flows intercellularly and intracellularly in through the ventral membrane and out through the apical membrane. In this more comprehensive model a third pathway for the currents is included, i.e., flow through the lateral membrane and out through the apical membrane. Inasmuch as tight junctions in epithelia result in higher junctional resistance than for fibroblast or endothelial cells, this third path is important to make model calculation of epithelial cells fit the experimental data, particularly in the high-frequency region.

After measuring the impedance of a confluent layer of Madin–Darby canine kidney (MDCK) cells (stain II) at various frequencies from 20 to 50,000 Hz by ECIS, a very good fit is obtained between the model calculation and the experimental data. We conclude that (1) junctional resistance of this leaky type of MDCK cell is 50~60 $\Omega \cdot cm^2$, (2) the distance between the ventral cell surface and substratum is less than 1 nm, and (3) the capacitance of apical, basal, and lateral cell membranes is 4.5, 3, and 1 $\mu F/cm^2$, respectively.

To verify this method further, we also measured the change in morphology of MDCK cells by first removing and then replacing Ca^{2+} ions in the culture medium. These data demonstrate that both tight junctions and cell–substratum interaction can be strongly and reversibly influenced by Ca^{2+}.

MATERIALS AND METHODS

Tissue culture

As a result of different passage numbers, there are two kinds of MDCK cell, referred to as strains I and II. Epithelia formed by strains I and II of MDCK cells show high (~4000-$\Omega \cdot cm^2$) and low (~80-$\Omega \cdot cm^2$) junctional resistance, respectively (Simmons, 1981; Handler, 1983; Fuller et al., 1984). In this study we used MDCK cells (strain II) obtained from ATCC (Rockville, MD). Cells were normally cultured at 37°C and 5% CO_2 in Dulbecco's modified Eagle's medium (GIBCO, Grand Island, NY) with 10% fetal bovine serum (GIBCO) and 50-μg/ml gentamicin. Inoculation of electrode-containing dishes was at 10^5 cells/cm^2. In experiments in which cells were deprived of calcium, cells were first grown to confluence in Dulbecco's modified Eagle's medium. After two to three days (after tight junctions had formed) the medium was changed to Earle's balanced salt solution (EBSS) with 1.8-mM Ca^{2+}. Twenty-four hours later the medium was changed to EBSS without Ca^{2+}. Following exposure of MDCK cells to a Ca^{2+}-free medium for 20 h, the Ca^{2+} containing EBSS was returned to the cells, and their recovery followed. All salt solutions contained normal levels of Mg^{2+}.

Electrode fabrication

Electrodes were fabricated by photolithography procedures essentially as previously described (Giaever and Keese, 1992); however, several modifications have recently been implemented. Gold was sputtered onto 20-mil polycarbonate sheets to produce an approximately 50-nm-thick film. These layers are thin enough to permit microscopic examination of the cell through the colored yet transparent metallic film. Following deposition of gold, a photolithographic procedure was used to delineate the desired gold patterns on the plastic substrate. A second photolithographic step was then used to produce 250-μm-diameter holes in a photoresist film; these are the active ECIS electrodes. To form tissue culture wells, 10-mm-diameter glass cylinders are mounted over each electrode pair with a silicone adhesive. The completed electrode arrays are cleaned and sterilized with an oxygen plasma etcher. The completed array consists of five sterile wells, each containing the ~250-μm-diameter electrode and a larger counterelectrode.

Impedance measurements

For impedance measurements the electrode arrays were placed in an incubator and a medium (0.5 ml) was added over the electrode in each well. The large electrode and one of the small electrodes were connected via a relay bank to a phase-sensitive lock-in amplifier, and an ac current was applied through a 1-MW load resistor (see Fig. 1). For monitoring cell motion and activities of MDCK cells, the measurement was generally carried out with an applied potential of 0.5 V at 700 Hz. For the frequency scans shown in Fig. 3 below, however, the following ac frequencies and respective amplitudes were used: 22 Hz and 0.12 V, 44 Hz and 0.12 V, 88 Hz and 0.12 V, 176 Hz and 0.12 V, 352 Hz and 0.12 V, 704 Hz and 0.151 V, 1408 Hz and 0.211 V, 2816 Hz and 0.295 V, 5632 Hz and 0.413 V, 11,264 Hz and 0.578 V, 22,528 Hz and 0.810 V, 45,056 Hz and 1.134 V.

All connections were made with coaxial cable to minimize any externally induced electrical noise. Cells were allowed to attach, spread, and organize for at least 24 h before any of the impedance measurements reported in this paper were taken.

Model derivation

The model that we used to calculate the specific impedance (impedance for a unit area) of a cell-covered electrode as a function of frequency, Z_c, is

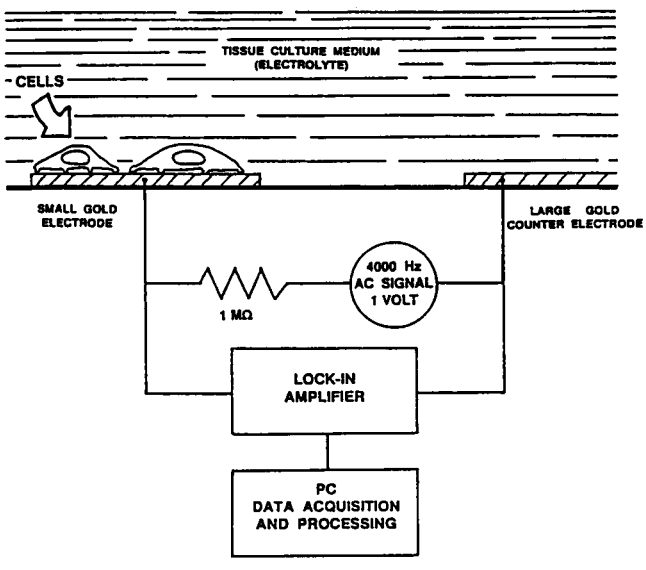

FIGURE 1 Schematic of the experimental setup. The lock-in amplifier is controlled by a computer that permits various modes of data collection. The 1-MW series resistance provides an approximately constant current source that make the measured in-phase voltage essentially proportional to resistance and the out-of-phase voltage proportional to reactance.

based on the measured values of a cell-free electrode, Z_n. The various current paths are sketched in Fig. 2. To make the calculations tractable, several simplifying assumptions must be made: 1) The cells are assumed to have a cylindrical shape with radius r_c, 2) the current flows radially in the space formed between the ventral surface of the cell and the substratum, and 3) the current density under the cells does not change in the vertical direction. 4) The electrode potential V_c is a constant that is independent of position, and 5) the potential in solution on the dorsal side of the cells is likewise treated as a constant, V_s (for convenience we set $V_s = 0$; this assignment will not affect the calculated impedance). Finally we assume 6) that the electrical potential inside the cells, V_i, is a constant and 7) that the presence of the cells does not affect the electrode polarization. The last simplifying assumption may not always be appropriate (Schwan, 1992).

The object is to use the measured impedance of a naked electrode, Z_n, to calculate the specific impedance of the cell-covered electrode, Z_c = (electrode area)$(V_c - V_s)/I_c = \pi r_c^2 V_c/I_{ct}$. I_c is the total current flowing from the electrode, I_{ct} is the current flowing from the area of a single cell, and the equation is true as long as we deal with confluent cell layers. Thus, if the current flowing from the area of a single cell can be calculated as a function of V_c, the problem is solved. From Fig. 2 we get by simply writing Ohm's law for an ac circuit

$$-\frac{dV}{dr} = \frac{\rho}{h2\pi r} I, \tag{1}$$

$$V_c - V = \frac{Z_n}{2\pi r\, dr} dI_c, \tag{2}$$

$$V - V_i = \frac{Z_b}{2\pi r\, dr} dI_i, \tag{3}$$

and

$$dI = dI_c - dI_i. \tag{4}$$

Equations 1–4 can be combined to yield the following differential equation

$$\frac{d^2V}{dr^2} + \frac{1}{r}\frac{dV}{dr} - \gamma^2 V + \beta = 0, \tag{5}$$

where

$$\gamma^2 = \frac{\rho}{h}\left(\frac{1}{Z_n} + \frac{1}{Z_b}\right), \tag{6}$$

and

$$\beta = \frac{\rho}{h}\left(\frac{V_c}{Z_n} + \frac{V_i}{Z_b}\right). \tag{7}$$

The general solution of Eq. 5 is

$$V = AI_0(\gamma r) + BK_0(\gamma r) + \frac{\beta}{\gamma^2}, \tag{8}$$

where $I_0(\gamma r)$ and $K_0(\gamma r)$ are modified Bessel functions of the first and second kinds, respectively. However, $K_0(\gamma r)$ goes to infinity as r goes to zero, and $r_c \geq r \geq 0$; hence, $B = 0$. Thus the solution of Eq. 5 is

$$V = AI_0(\gamma r) + \frac{\beta}{\gamma^2}. \tag{9}$$

For the intercellular lateral path the two equations related to the paracellular current can be expressed as

$$\frac{dV_l}{dz} = -2I_l R_l, \tag{10}$$

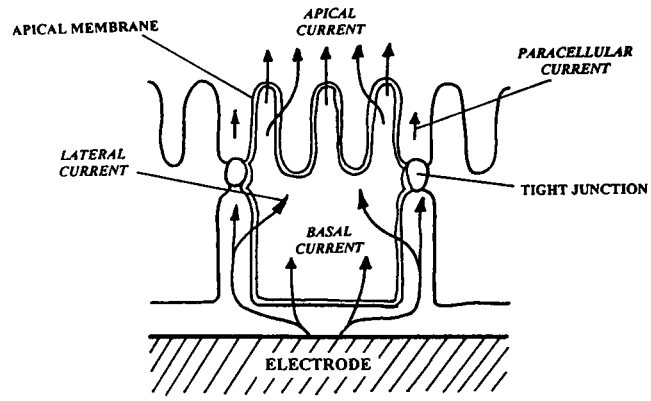

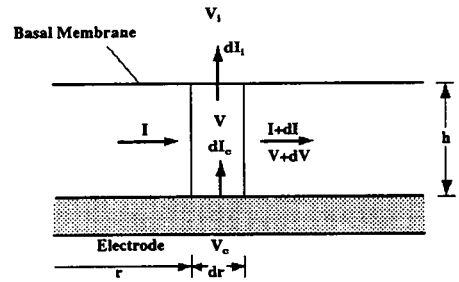

FIGURE 2 Schematic diagram of MDCK cells in tissue culture, illustrating the various current paths. The cells are regarded as disk shaped when viewed from the top, and the schematic side view diagram of cells is useful in constructing the differential equations, Eqs. 5 and 12. The increased impedance of a cell-covered electrode is in large part due to the current flow under the cells and comes in addition to the transcellular and paracellular pathways.

and

$$V_l - V_i = \frac{Z_l}{2\pi r_c dz}(-dI_l). \tag{11}$$

By combining Eqs. 10 and 11 we obtain the following differential equation

$$\frac{d^2V_l}{dz^2} - \lambda^2 V_l + \lambda^2 V_i = 0, \tag{12}$$

where

$$\lambda = \left(\frac{4\pi r_c R_l}{Z_l}\right)^{1/2}. \tag{13}$$

The solution of Eq. 12 is

$$V_l = V_i + Ce^{\lambda z} + De^{-\lambda z}. \tag{14}$$

We have four constants, A, C, D, and V_i, that must be determined, and the four boundary conditions are

$$V(r = r_c) = V_l(z = 0), \tag{15}$$

$$I(r = r_c) = I_l(z = 0), \tag{16}$$

$$I_l(z = l) \times R_b^* = V_l(z = l), \tag{17}$$

and

$$I_c = I_i + I_l(z = l). \tag{18}$$

It is straightforward to solve these equations in closed form, but the answers are rather complex. By using matrix algebra, which is part of many computer programs, a numerical solution can be readily obtained. Symbolically we may write

$$M\mathbf{X} = \mathbf{Y} \qquad \mathbf{X} = M^{-1}\mathbf{Y},$$

where **X** and **Y** are two vectors and the matrix M^{-1} is the inverse of the matrix M. From the four boundary conditions we obtain the following matrix equation

$$\begin{pmatrix} \dfrac{-2\pi h\gamma r_c I_1(\gamma r_c)}{\rho} & \dfrac{\lambda}{2R_l} & \dfrac{-\lambda}{2R_l} & 0 \\ I_0(\gamma r_c) & -1 & -1 & \dfrac{-Z_b}{Z_n + Z_b} \\ 0 & e^{\lambda l}\left(1 + \dfrac{\lambda R_b}{2R_l}\right) & e^{-\lambda l}\left(1 - \dfrac{\lambda R_b}{2R_l}\right) & 1 \\ \dfrac{-2I_1(\gamma r_c)}{Z_n \gamma r_c} & \dfrac{\lambda e^{\lambda l}}{2R_l \pi r_c^2} & \dfrac{-\lambda e^{-\lambda l}}{2R_l \pi r_c^2} & \dfrac{-(Z_a + Z_b + Z_n)}{(Z_n + Z_b)Z_a} \end{pmatrix} \begin{bmatrix} A \\ C \\ D \\ V_i \end{bmatrix} = \begin{bmatrix} 0 \\ \dfrac{-V_c Z_b}{Z_n + Z_b} \\ 0 \\ \dfrac{-V_c}{Z_n + Z_b} \end{bmatrix}. \tag{19}$$

The numerical constants *A*, *C*, *D*, and V_i are found by solving this equation, and finally the current flowing out of the electrode under a single cell can be found by integrating Eq. 2:

$$\begin{aligned} I_{ct} &= \int_0^{rc} \frac{2\pi r}{Z_n}(V_c - V)\, dr \\ &= \frac{-2\pi r_c^2 A}{Z_n \gamma r_c} I_1(\gamma r_c) + \frac{\pi r_c^2}{Z_n + Z_b}(V_c - V_i), \end{aligned} \tag{20}$$

and the impedance is obtained by dividing V_c by I_{ct}.

RESULTS

Model analysis of ECIS

Fig. 3*a* and *b* plot the resistance and capacitance of the transepithelial impedance as a function of frequency. Both of these figures show experimental data for cell-free electrodes and electrodes confluent with MDCK cells (strain II) measured in the complete medium, and calculated values (points). Fig. 4*a* and *b* display normalized resistance and capacitance obtained by dividing the impedance values from electrodes confluent with MDCK cells by the corresponding quantities for the cell-free electrodes.

The calculated values are based on the impedance of the naked electrode. Because the solution resistance (constriction resistance) is a significant part of the measured impedance, it must first be subtracted from the measured impedance before the calculations are done and then added back for comparison with the experimental results (Giaever and Keese, 1991). The numerical value of the constriction resistance is simply equal to the asymptotic value at high frequency of the measured resistance for a cell-free electrode. In addition we have assumed that the specific membrane resistance, R_m, of the cells is 1000 $\Omega\cdot cm^2$, and because this is large compared with the reactance $1/2\pi\nu C_m$ at most frequencies it has little effect on the results. (The membrane impedance, Z_m, is $1/Z_m = (1/R_m) + i2\pi\nu C_m$).

To get a feel for how the many parameters affect the result we shall do a few model calculations. Fig. 5*a* and *b* show the normalized resistance and capacitance as a function of frequency for a range of R_b values 20, 40, 60, and 80 $\Omega\cdot cm^2$, with $\alpha = 20\ \Omega^{1/2}\cdot cm$, $C_a = 4\ \mu F/cm^2$, and $C_b = 3$

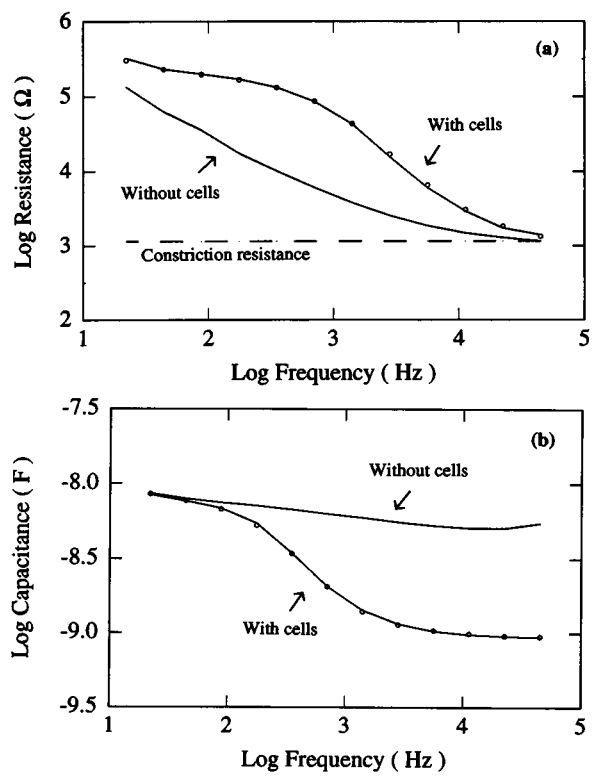

FIGURE 3 (*a*) Resistance and (*b*) capacitance as a function of frequency obtained from frequency scan measurement for an electrode with and without a monolayer of MDCK cells. The points are calculated values based on the measured impedance of the cell-free electrode and using the model in this paper. Note that the resistance is a sum of the electrode resistance and the frequency-independent solution resistance (constriction resistance). At low frequency the electrode resistance dominates, and at high frequency the constriction resistance dominates.

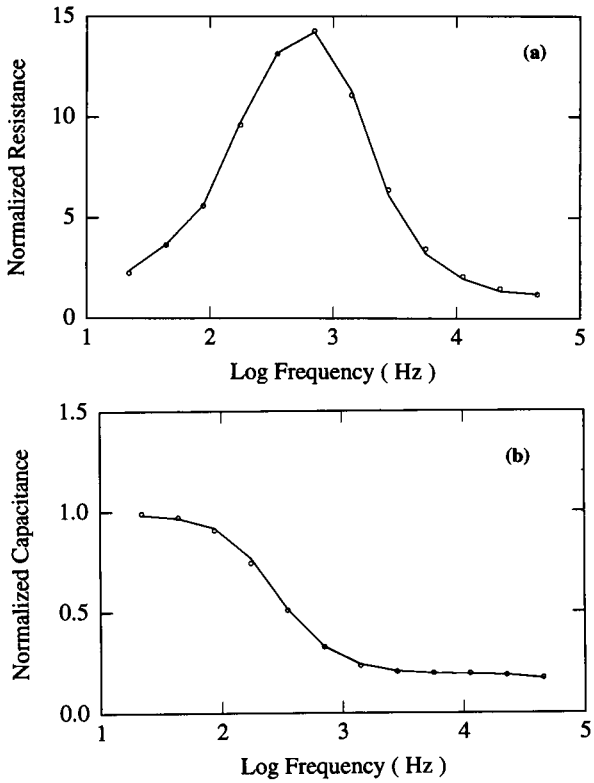

FIGURE 4 (*a*) Normalized resistance and (*b*) normalized capacitance for an electrode with a confluent MDCK cell layer. The curves are obtained from Fig. 3 by dividing the measured values of the cell-covered electrode by the corresponding values of the cell-free electrode. Again the points are calculated values. The reason for the peak is that the constriction resistance masks the electrode resistance at high frequency.

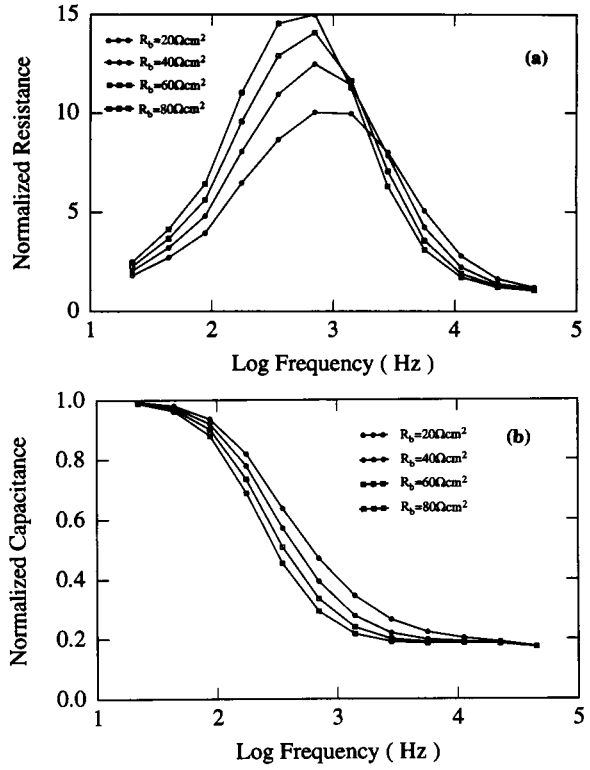

FIGURE 5 (*a*) Normalized resistance and (*b*) normalized capacitance from model calculation for different junctional resistances (R_b) corresponding to 20, 40, 60, and 80 $\Omega{\cdot}cm^2$. The other parameters, α, C_a, and C_b, were set to be 20 $\Omega^{1/2}{\cdot}cm$, 4 $\mu F/cm^2$, and 3 $\mu F/cm^2$ respectively; these values are close to the experimental results of MDCK cells.

$\mu F/cm^2$. When R_b increases, the low-frequency values of the normalized resistance increase while the high-frequency values decrease. Fig. 6*a* and *b* show another calculation, where α takes the values of 10, 20, 30, and 40 $\Omega^{1/2}{\cdot}cm$, $R_b = 60\ \Omega{\cdot}cm^2$, and C_a and C_b have the same values as in Fig. 5. Finally, Fig. 7*a* and *b* show a third calculation, where C_a takes the values of 1, 2, 3, and 5 $\mu F/cm^2$, $R_b = 60\ \Omega{\cdot}cm^2$, $\alpha = 20\ \Omega^{1/2}{\cdot}cm$, and $C_b = 3\ \mu F/cm^2$. Because C_a and C_b are in series, changes in C_b only rather than in C_a give similar results. This is not true when we consider the lateral membrane capacitance C_l, which becomes important when R_b is large. In general, values for C_b and C_l that give the best fit to experimental data will be smaller than the value used for C_b above.

Because many parameters need to be adjusted, it is convenient when fitting experimental data to start by ignoring the lateral impedance. After reasonable values of R_b, α, C_a, and C_b are obtained, R_l and C_l can be used for fine tuning to arrive at the best fit.

Values for MDCK cells

We analyzed the transepithelial impedance of confluent MDCK cell layers as described above. The best fit obtained with four parameters is R_b, α, C_a, and C_b at 62 $\Omega{\cdot}cm^2$, 20 $\Omega^{1/2}{\cdot}cm$, 5 $\mu F/cm^2$, and 3 $\mu F/cm^2$ respectively. From another report (Cereijido et al., 1983) we know that the approximate radius and thickness of MDCK cells are 7 and 5 μm, respectively. The area of lateral cell membrane is then easily calculated, and the best fits of R_b, α, C_a, C_b, and C_l are 62 $\Omega{\cdot}cm^2$, 19 $\Omega^{1/2}{\cdot}cm$, 4.5 $\mu F/cm^2$, 3.0 $\mu F/cm^2$, and 1.0 $\mu F/cm^2$ respectively. However, the value 62 $\Omega{\cdot}cm^2$ includes the lateral paracellular resistance between the cells. To calculate R_l we assume that the width of the intercellular lateral space is 15~20 nm (Geiger et al., 1985). The final results of R_b, α, C_a, C_b, and C_l for a MDCK (strain II) confluent cell layer are 55 $\Omega{\cdot}cm^2$, 18 $\Omega^{1/2}{\cdot}cm$, 4.5 $\mu F/cm^2$, 3.0 $\mu F/cm^2$, and 1.0 $\mu F/cm^2$, respectively. This junctional resistance R_b is similar to those values from transepithelial resistance measurements obtained, for example, by Richardson et al. (1981) and Stevenson et al. (1988b). Because $\alpha = r_c(\rho/h)^{1/2}$, by using the values of α and r_c described above and because ρ is measured to be 54 $\Omega{\cdot}cm$, we can calculate the average height between basal cell surface and substratum and get the average h of roughly 1 nm. This distance is surprisingly small, implying that the ventral surfaces of the cell and the substratum are essentially in contact.

Ca^{2+} Removal and addition

Following transepithelial impedance measurement for MDCK cells in the complete medium, we replaced the

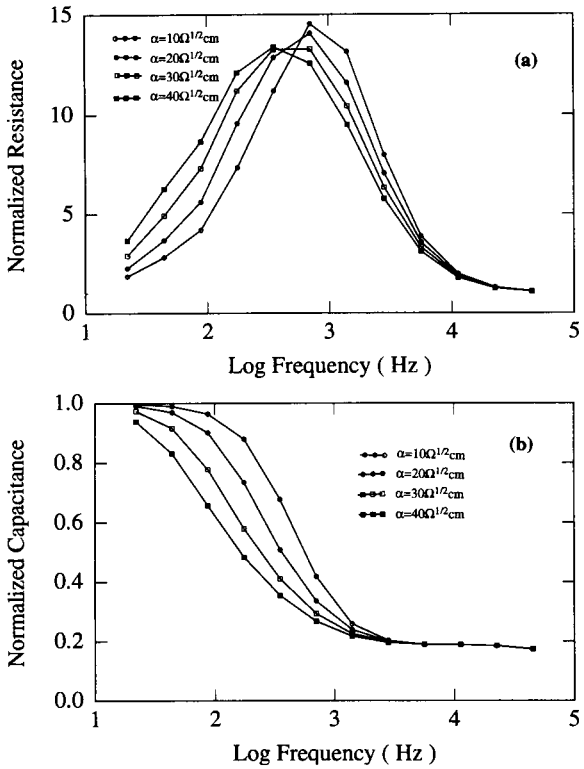

FIGURE 6 (*a*) Normalized resistance and (*b*) normalized capacitance from model calculation for different parameters α corresponding to 10, 20, 30, and 40 $\Omega^{1/2}$·cm. The other parameters, R_b, C_a, and C_b, were set to be 60 Ω·cm^2, 4 μF/cm^2, and 3 μF/cm^2 respectively.

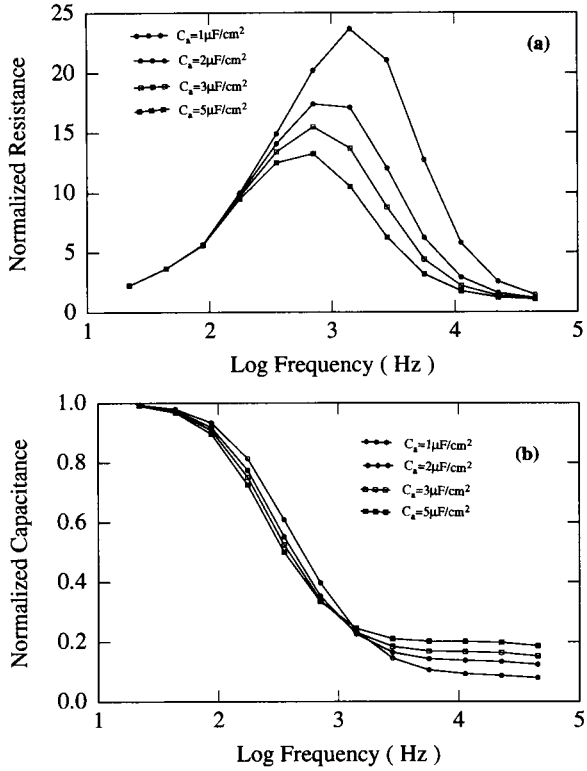

FIGURE 7 (*a*) Normalized resistance and (*b*) normalized capacitance from model calculation for different apical membrane capacitances (C_a) corresponding to 1, 2, 3, and 5 μF/cm^2. The other parameters, R_b, α, and C_b, were set to be 60 Ω·cm^2, 20 $\Omega^{1/2}$·cm, and 3 μF/cm^2, respectively.

medium with Earle's balanced salt solution (EBSS) containing 1.8-mM Ca^{2+}. After 24 h in Earle's balanced salt solution the transepithelial impedance did not change significantly, and all morphological parameters from impedance analysis were similar to those obtained from cells in complete Dulbecco's modified Eagle's medium. However, when the medium was changed to EBSS without Ca^{2+}, both the junctional resistance R_b and the parameter α (obtained from data fitting) dropped quickly, as shown in Fig. 8 (filled circles). Twenty hours later, when R_b and α had decreased to 0.8 Ω·cm^2 and 3.5 $\Omega^{1/2}$·cm, respectively, EBSS without Ca^{2+} was again replaced with EBSS containing 1.8-mM Ca^{2+}. As shown by Fig. 8 (open circles), the junctional resistance R_b and the parameter α increased slowly in the first few hours and then more quickly for a complete recovery in approximately 20 h. Fig. 9 illustrates how the average height (h) (calculated from α) between the basal cell surface and the substratum depends on the removal (filled circles) and replacement (open circles) of Ca^{2+} in the medium.

DISCUSSION

Transepithelial impedance measurement using the ECIS technique is a simple method for studying the transport and morphological properties of epithelia. It is easy to culture cells on the electrodes, the measurements are not time consuming, and, although the interpretation may seem complex, it is a straightforward numerical calculation with the developed model.

Different cell types display different impedances as a function of frequency. The peak value of the normalized resistive curve in Fig. 3 *a*, for MDCK cells approximately 15 at 700 Hz, is quite different from that for fibroblastic cells, i.e., WI-38 VA13 cells, for which the peak value of the normalized resistance is 6 at approximately 4000 Hz (Giaever and Keese, 1991). The shift in the peak results basically from increases in both R_b and α, as shown in Figs. 5 *a* and 6 *a*. Compared to WI-38 VA13 fibroblasts, MDCK cells have a larger junctional resistance and are spaced much closer to the substratum, based on model calculations. The capacitive values of the cell membranes obtained from data fitting indicate that the apical cell surface of a MDCK cell (strain II) has more folds than the basal membrane and that the lateral cell membrane is the least convoluted. As seen, the developed model can be made to fit the data very well. Whereas fibroblastic and most other cells without tight junctions can be fitted very well with only three parameters, i.e., R_b, α, and C_a, it is necessary to use all the parameters to get a similarly good fit for cells with tight junctions. Because of the simplicity of the ECIS instrumental system and the good agreement between theory and experiment, we expect that impedance analysis of cells by ECIS will find many applications in the future.

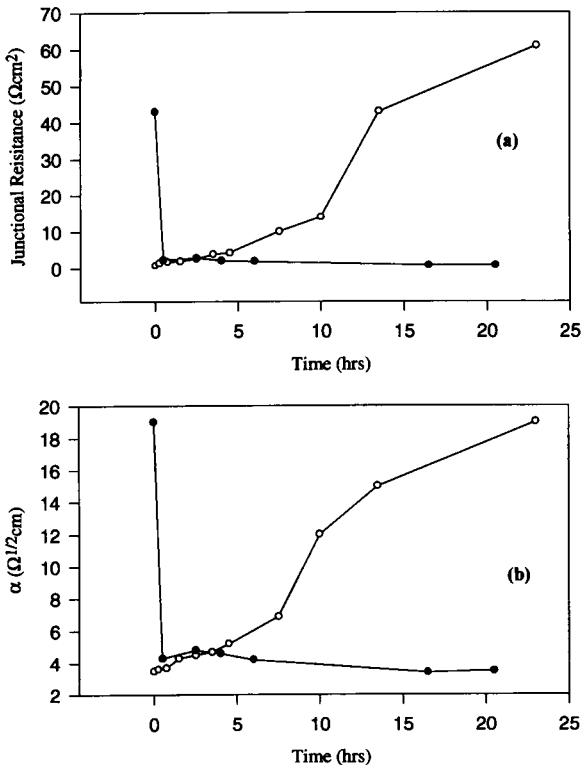

FIGURE 8 Change in (*a*) junctional resistance and (*b*) parameter α as a function of time during Ca^{2+} removal (filled circles) and replacement (open circles).

When Ca^{2+} is removed and then added back to the medium, opening and resealing of the tight junctions causes the junctional resistance to decrease and then recover (Cereijido et al., 1978; Gonzalez-Mariscal et al., 1990; Contreras et al., 1991). The data shown in Fig. 8 *a* confirm this. Furthermore, the ECIS experimental results also demonstrate that, in addition, the parameter α decreases in a Ca^{2+}-free medium, as shown in Fig. 8 *b*. Data (not shown) suggest that changes in Ca^{2+} concentration do not result in significant changes in the capacitance of the cell membranes

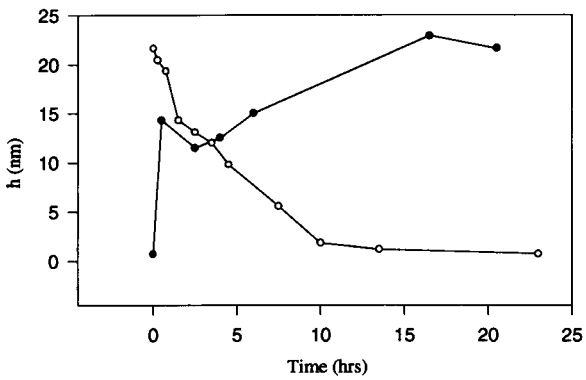

FIGURE 9 Average height (h) between basal cell surface and substratum as a function of time during Ca^{2+} removal (filled circles) and replacement (open circles).

or in the average radius of the individual cells. As a result, changes in parameter α must be attributable mainly to changes in the spacing between the cells and their substratum. Using the relation $\alpha = r_c(\rho/h)^{1/2}$, we calculated the average height between the basal cell surface and substratum (h) as shown in Fig. 9. This average height changed from approximately 1 to 22 nm as MDCK cells were cultured in Ca^{2+}-free EBSS for 20 h. Because the specific role of Ca^{2+} in cell-substratum adhesion is not well known, the method provided here may be an important way to study the mechanisms of cell-substratum adhesion.

APPENDIX

List of Symbols

Z_n ($\Omega\cdot cm^2$)	specific impedance (impedance for a unit area) of the cell-free electrode
Z_a ($\Omega\cdot cm^2$)	specific impedance through the apical cell membrane
Z_b ($\Omega\cdot cm^2$)	specific impedance through the basal cell membrane
Z_l ($\Omega\cdot cm^2$)	specific impedance through the lateral cell membrane
Z_c ($\Omega\cdot cm^2$)	specific impedance of the cell-covered electrode
V_c (V)	applied voltage across the cell
V_i (V)	potential inside the cell
V_l (V)	potential in the lateral paracellular path
I_c (A)	total current across the cell-covered electrode
I_{ct} (A)	total current from the area of a single cell
I_i (A)	transcellular current through the apical cell surface
I_l (A)	paracellular current through the intercellular lateral path
R_l ($\Omega\cdot cm^{-1}$)	lateral paracellular resistance for a unit length
R_b* (Ω)	junctional resistance between adjacent cells
R_b ($\Omega\cdot cm^2$)	junctional resistance between adjacent cells over a unit cell area
ρ ($\Omega\cdot cm$)	resistivity of the cell culture medium
r_c (μm)	cell radius
l (μm)	length of the lateral paracellular path
h (nm)	height between the basal cell surface and the substratum

REFERENCES

Boulpaep, E. L., and H. Sackin. 1980. Electrical analysis of intraepithelial barriers. *Curr. Top. Membr. Transp.* 13:169–197.

Cereijido, M., E. S. Robbins, W. J. Dolan, C. A. Rotunno, and D. D. Sabatini. 1978. Polarized monolayers formed by epithelial cells on a permeable and translucent support. *J. Cell Biol.* 77:853–880.

Cereijido, M., L. Gonzalez-Mariscal, and L. Borboa. 1983. Occluding junctions and paracellular pathways studied in monolayers of MDCK cells. *J. Exp. Biol.* 106:205–215.

Cereijido, M., L. Gonzalez-Mariscal, G. Avila, and R. G. Contreras. 1988. Tight junctions. *CRC Crit. Rev. Anat. Sci.* 1:171–192.

Claude, P. 1978. Morphological factors influencing transepithelial permeability: a model for the resistance of the zonula occludens. *J. Membr.Biol.* 39:219–232.

Clausen, C., S. A. Lewis, and J. M. Diamond. 1979. Impedance analysis of a tight epithelium using a distributed resistance model. *Biophys. J.* 26:291–318.

Clausen, C. 1989. Impedance analysis in tight epithelia. *Meth. Enzymol.* 171:628–642.

Cole, K. S. 1968. Membranes, Ions and Impulses. University of California Press, Berkeley. 12 pp.

Contreras, R. G., A. Ponce, and J. J. Bolivar. 1991. Calcium and tight junctions. *In* Tight Junctions. M. Cereijido, editor. CRC, Boca Raton, FL. 139–149.

Conyers, G., L. Milks, M. Conklyn, H. Showell, and E. Cramer. 1990. A factor in serum lowers resistance and opens tight junctions of MDCK cells. *Am. J. Physiol.* 259:C577-C585.

Fromter, E. 1972. The route of passive ion movement through the epithelium of *Necturus* gallbladder. *J. Membr. Biol.* 8:259–301.

Fromter, E., and J. M. Diamond. 1972. Route of passive ion permeation in epithelia. *Nature New Biol.* 235:9–13.

Fuller, S., C.-H. von Bonsdorff, and K. Simons. 1984. Vesicular stomatitis virus infects and matures only through the basolateral surface of the polarized epithelial cell line, MDCK. *Cell.* 38:65–77.

Geiger, B., Z. Avnur, T. Volberg, and T. Volk. 1985. Molecular domains of adherens junctions. *In* The cell in Contact. G. M. Edelman and J.-P. Thiery, editors. John Wiley & Sons, New York. 461–489.

Giaever, I., and C. R. Keese. 1984. Monitoring fibroblast behavior in tissue culture with an applied electric field. *Proc. Natl. Acad. Sci. (USA).* 81:3761–3764.

Giaever, I., and C. R. Keese. 1986. Use of electric fields to monitor the dynamical aspect of cell behavior in tissue culture. *IEEE Trans. Biomed. Eng.* 33:242–247.

Giaever, I., and C. R. Keese. 1991. Micromotion of mammalian cells measured electrically. *Proc. Natl. Acad. Sci.(USA).* 88:7896–7900.

Giaever, I., and C. R. Keese. 1992. Toxic? Cells can tell. *Chemtech.* Feb. 116–125.

Giaever, I., and C. R. Keese 1993. Correction *Proc. Natl. Acad. Sci.(USA).* 90 1634.

Gonzalez-Mariscal, L., R. G. Contreras, J. J. Bolivar, A. Ponce, B. Chavez de Ramirez, and M. Cereijido. 1990. Role of calcium in tight junction formation between epithelial cells. *Am. J. Physiol.* 259:C978-C986.

Gordon, L. G. M., G. Kottra, and E. Fromter. 1989. Electrical impedance analysis of leaky epithelia: theory, techniques, and leak artifact problems. *Meth. Enzymol.* 171:642–663.

Gumbiner, B. 1987. Structure, biochemistry, and assembly of epithelial tight junctions. *Am. J. Physiol.* 253:C749-C758.

Gumbiner, B., and K. Simons. 1986. A functional assay for proteins involved in establishing an epithelial occluding barrier: identification of a uvomorulin-like polypeptide. *J. Cell Biol.* 102:457–468.

Handler, J. S. 1983. Use of cultured epithelia to study transport and its regulation. *J. Exp. Biol.* 106:55–69.

Lewis, S. A., and J. M. Diamond. 1976. Na^+ transport by rabbit urinary bladder, a tight epithelium. *J. Membr. Biol.* 28:1–40.

Lim, J. J., G. Kottra, L. Kampmann, and E. Fromter. 1984. Impedance analysis of *Necturus* gallbladder epithelium using extra- and intracellular microelectrodes. *Curr. Top. Membr. Transp.* 20:27–46.

Lo, C. -M., C. R. Keese, and I. Giaever. 1993. Monitoring motion of confluent cells in tissue culture. *Exp. Cell Res.* 204:102–109.

Madara, J. L. 1988. Tight junction dynamics: is paracellular transport regulated? *Cell.* 53:497–498.

Madara, J. L., and J. R. Pappenheimer. 1987. Structural basis for physiological regulation of paracellular pathways in intestinal epithelia. *J. Membr. Biol.* 100:149–164.

Pappenheimer, J. R. 1987. Physiological regulation of transepithelial impedance in the intestinal mucosa of rats and hamsters. *J. Membr. Biol.* 100:137–148.

Powell, D. W. 1981. Barrier function of epithelia. *Am. J. Physiol.* 241: G275-G288.

Reuss, L. 1991. Tight junction permeability to ions and water. *In* Tight Junctions. M. Cereijido, editor. CRC, Boca Raton, FL. 49–66.

Richardson, J. C. W., V. Scalera, and N. L. Simmons. 1981. Identification of two strains of MDCK cells which resemble separate nephron tubule segments. *Biochim. Biophys. Acta.* 673:26–36.

Schwan, H. P. 1992. Linear and nonlinear electrode polarization and biological materials. *Ann. Biomed. Eng.* 20:269–288.

Simmons, N. L. 1981. Ion transport in tight epithelial monolayers of MDCK cells. *J. Membr. Biol.* 59:105–114.

Stevenson, B. R., J. M. Anderson, and S. Bullivant. 1988a. The epithelial tight junction: structure, function, and preliminary biochemical characterization. *Mol. Cell. Biochem.* 83:129–145.

Stevenson, B. R., J. M. Anderson, D. A. Goodenough, and M. S. Mooseker. 1988b. Tight junction structure and ZO-1 content are identical in two strains of Madin-Darby canine kidney cells which differ in transepithelial resistance. *J. Cell Biol.* 107:2401–2408

Wills, N. K., and C. Clausen. 1987. Transport-dependent alterations of membrane properties of mammalian colon measured using impedance analysis. *J. Membr. Biol.* 95:21–35.